JCI insight

RESEARCH ARTICLE

Obesity-induced hepatic steatosis is mediated by endoplasmic reticulum stress in the subfornical organ of the brain

Julie A. Horwath,[1,2] Chansol Hurr,[3] Scott D. Butler,[1] Mallikarjun Guruju,[2] Martin D. Cassell,[4] Allyn L. Mark,[2,5] Robin L. Davisson,[1,2] and Colin N. Young[3]

[1]Biomedical Sciences, College of Veterinary Medicine, Cornell University, Ithaca, New York, USA. [2]Cell and Developmental Biology, Weill Cornell Medical College, New York, New York, USA. [3]Pharmacology and Physiology, School of Medicine and Health Sciences, The George Washington University, Washington, DC, USA. [4]Anatomy and Cell Biology, University of Iowa, Iowa City, Iowa, USA. [5]Internal Medicine, University of Iowa, Iowa City, Iowa, USA.

Nonalcoholic fatty liver disease (NAFLD), characterized by an excess accumulation of hepatic triglycerides, is a growing health epidemic. While ER stress in the liver has been implicated in the development of NAFLD, the role of brain ER stress — which is emerging as a key contributor to a number of chronic diseases including obesity — in NAFLD remains unclear. These studies reveal that chemical induction of ER stress in the brain caused hepatomegaly and hepatic steatosis in mice. Conversely, pharmacological reductions in brain ER stress in diet-induced obese mice rescued NAFLD independent of body weight, food intake, and adiposity. Evaluation of brain regions involved revealed robust activation of ER stress biomarkers and ER ultrastructural abnormalities in the circumventricular subfornical organ (SFO), a nucleus situated outside of the blood-brain-barrier, in response to high-fat diet. Targeted reductions in SFO-ER stress in obese mice via SFO-specific supplementation of the ER chaperone 78-kDa glucose–regulated protein ameliorated hepatomegaly and hepatic steatosis without altering body weight, food intake, adiposity, or obesity-induced hypertension. Overall, these findings indicate a novel role for brain ER stress, notably within the SFO, in the pathogenesis of NAFLD.

Introduction

Nonalcoholic fatty liver disease (NAFLD) affects approximately a third of the population in Western societies and is directly associated with the incidence of obesity (1–3). Striking population-based studies indicate that upwards of 75% of obese and morbidly obese adults are affected by NAFLD (2). Considered to be the hepatic manifestation of the metabolic syndrome, NAFLD encompasses a spectrum of liver damage beginning with the excess accumulation of triglycerides in the liver (i.e., steatosis). Steatosis, in turn, can progress to nonalcoholic steatohepatitis (NASH), fibrosis, cirrhosis, and hepatocellular carcinoma (1, 3, 4). In addition to detrimental hepatic consequences, individuals with NAFLD are at an increased risk for the development of type II diabetes, hypertension, insulin resistance, and obesity-related mortality (5–7). Understanding the underlying mechanisms contributing to NAFLD is a priority, with accumulating evidence implicating disruptions in ER homeostasis as central to the development of hepatic steatosis and NAFLD (8–12).

As the primary site of cellular protein folding, maturation, processing, and transport, the ER plays a critical role in maintaining appropriate cellular function. In situations such as nutritional excess, where the protein load exceeds the ER folding capacity, a collection of conserved signaling pathways, termed the unfolded protein response (UPR), are activated as a homeostatic mechanism to preserve ER function. While beneficial in the short-term, chronic UPR activation, known as ER stress, is now recognized as a major pathological mechanism in a variety of metabolic diseases, including obesity (8, 9, 12–14). In the context of NAFLD, genetic and diet-induced obesity (DIO) in rodent models have been shown to be associated with hepatic ER stress (11, 15). Since these initial observations, a growing body of literature from obese animal models and patients with NAFLD supports a causal role for hepatic ER stress in NAFLD (8–10). Moreover, ER stress is linked to a number of sequelae, which are common in NAFLD, including insulin resistance, inflammation, lipotoxicity, and oxidative stress (8, 9, 13, 14, 16).

Conflict of interest: The authors have declared that no conflict of interest exists.

Submitted: August 18, 2016
Accepted: March 2, 2017
Published: April 20, 2017

Reference information:
JCI Insight. 2017;2(8):e90170. https://doi.org/10.1172/jci.insight.90170.

Importantly, the CNS also plays a critical role in the modulation of energy homeostasis through neuronal networks that sense and integrate a variety of circulating (e.g., insulin) and local (e.g., neuropeptide) signals (17–19). Despite indications that the CNS is involved in hepatic lipid metabolism, very low-density lipoprotein assembly and secretion, gluconeogenesis, and glyogenolysis (18–20), the extent to which dysregulation in brain signaling contributes to NAFLD remains unclear. Interestingly, obesity is associated with the development of brain as well as hepatic ER stress (21–23). However, investigation of the functional role of CNS ER stress in the context of obesity has been focused mostly on feeding behavior and adipose tissue metabolism, not hepatic parameters (22, 23).

Here, we tested the hypothesis that CNS ER stress is a key contributor to obesity-induced NAFLD. Our findings demonstrate that brain UPR activation, notably within the forebrain subfornical organ (SFO), a tiny circumventricular region situated outside of the blood-brain-barrier, is causally linked to hepatic steatosis during DIO.

Results

Acute chemical induction of brain ER stress promotes hepatic steatosis independent of body weight, food intake, or adiposity. While ER stress in the CNS is emerging as a key controller of metabolic processes, the extent to which it is involved in NAFLD remains unknown. To investigate this, we first examined the effects of selective induction of ER stress in the brain on hepatic parameters. Adult C57Bl/6 mice on normal chow were preimplanted with an intracerebroventricular (ICV) cannula in the lateral ventricle, and the chemical ER stress inducer thapsigargin was subsequently administered ICV once daily over 3 days. Consistent with previous reports (21, 24), this approach evoked robust UPR activation in the CNS (Supplemental Figure 1; supplemental material available online with this article; https://doi.org/10.1172/jci.insight.90170DS1), particularly within forebrain and hindbrain regions. Short-term ICV administration of thapsigargin resulted in hepatomegaly (~25% increase in liver weight; Figure 1A) and an almost 4-fold increase in liver triglycerides (Figure 1B). In addition, histological examination of the liver revealed substantial steatosis (Figure 1C), as represented by vacuolation and lipid droplet accumulation in hepatocytes, in mice treated with ICV thapsigargin. In contrast, induction of brain ER stress did not influence body weight, food intake, or regional adipose tissue mass (Figure 1, D–G). Importantly, ICV thapsigargin did not alter hepatic ER stress markers (Supplemental Figure 2), demonstrating that these findings are due to UPR activation in the brain and not in the liver. This indicates that acute brain ER stress can cause hepatic steatosis, independent of changes in body weight, food intake, adiposity, and hepatic ER stress.

Short-term reduction in brain ER stress rescues obesity-induced hepatic steatosis without affecting body weight, food intake, or adiposity. Next, we asked if chronic brain ER stress, such as that which occurs in DIO, contributes to fatty liver. In C57Bl/6 mice with DIO induced by a high-fat diet (HFD) for 15 weeks, we utilized short-term ICV administration of taurosdeoxycholic acid (TUDCA), an ER chemical chaperone that reduces brain ER stress (21, 22, 24). As expected, significant elevations in liver weight (i.e., hepatomegaly; Figure 2A) were observed following HFD feeding. Remarkably, obesity-induced hepatomegaly was restored to normal chow levels following ICV TUDCA over 3 days (Figure 2B). Moreover, while HFD-fed animals treated with ICV vehicle demonstrated profound elevations in liver triglycerides and hepatic lipid vesicle accumulation, 3-day ICV brain administration of TUDCA reduced HFD-induced hepatic steatosis and restored liver histology to a normal appearance (Figure 2, B and C). Importantly, ICV TUDCA did not alter mRNA levels of hepatic ER stress markers in DIO or normal-chow mice (Supplemental Figure 3A). As anticipated, HFD resulted in significant elevations in body weight and regional adipose tissue mass, but reducing brain ER stress via ICV TUDCA over 3 days did not influence these parameters or food intake (Figure 2, D–G). Collectively, these findings demonstrate that CNS ER stress underlies hepatic steatosis during obesity, and this effect is dissociated from body weight, adiposity, food intake, and hepatic ER stress.

Short-term reductions in brain ER stress rescue hypertension and tachycardia in DIO mice. Activation of the UPR in the CNS is also emerging as an important contributor to cardiovascular diseases, including hypertension (21, 24). In this context, we and others have previously shown that acute induction of brain ER stress (ICV thapsigargin) increases arterial blood pressure (21, 24). Since obesity is associated with the development of hypertension (25, 26), we also determined the contribution of brain ER stress to obesity-induced hypertension. Using radiotelemetric analyses, HFD-fed animals were found to have significant elevations in arterial pressure, as well as tachycardia (Figure 2, H and I). ICV administration of TUDCA over 3 days lowered arterial pressure and heart rate in DIO mice, a response that was evident within 24–48

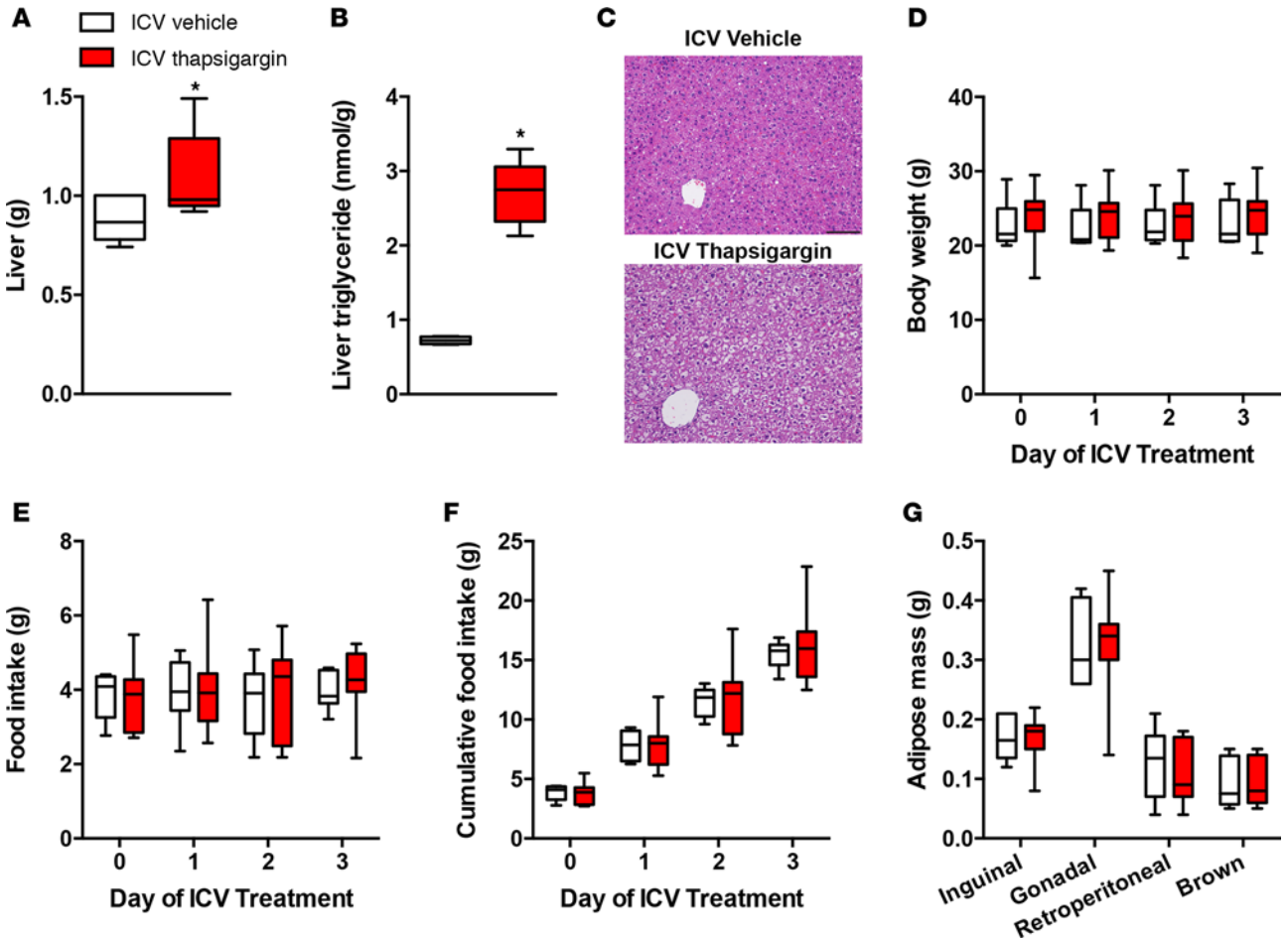

Figure 1. Short-term induction of brain ER stress promotes hepatic steatosis independent of changes in body weight, food intake, or adiposity. Liver mass (**A**) and hepatic triglyceride levels (**B**) following 3 days of daily intracerebroventricular (ICV) vehicle or thapsigargin (to induce brain ER stress) administration. n = 6–10. (**C**) H&E staining of the liver in mice that underwent ICV vehicle or thapsigargin dosing. Representative of n = 4. Scale bar: 100 μm. Body weight (**D**), food intake (**E**), and cumulative food intake (**F**) at baseline and during 3 days of daily ICV vehicle or thapsigargin administration. Regional adipose tissue mass (**G**) following 3 days of ICV vehicle or thapsigargin. n = 6–10. *P < 0.05 vs. ICV vehicle with two-tailed unpaired t-test or 2-way repeated measures ANOVA. Box-and-whisker plots represent the median (line within box), upper and lower quartile (bounds of box), and maximum and minimum values (bars).

hours, with blood pressure and heart rate in ICV TUDCA–treated DIO mice returning to normal chow levels within 72 hours (Figure 2, H and I). Thus, brain ER stress contributes to obesity-induced hypertension, an abnormality that commonly occurs in concert with NAFLD (27, 28).

Obesity elicits robust UPR activation and ER ultrastructural abnormalities in the SFO. We subsequently sought to determine the neural regions involved in the CNS ER stress–mediated responses in DIO mice. In light of our findings of ER stress–mediated cardiovascular and metabolic effects (Figure 2, A–C, H, and I), we focused our attention on the sensory circumventricular SFO. This tiny forebrain CNS nucleus located at the base of the lateral ventricle is highly vascularized and lacks a blood-brain-barrier (Figure 3A), unlike the vast majority of brain regions, including the hypothalamus (29–31). This unique feature makes the SFO highly susceptible to ER stress during obesity due to its constant exposure to circulating metabolites, hormones, and inflammatory mediators. Well known for its role in fluid and cardiovascular homeostasis, an emerging body of evidence suggests that the SFO may also be intricately involved in metabolic control and serve as a central integrator to couple metabolic and cardiovascular responses (30, 32, 33).

We first performed gene expression of the ER stress indicators *p58IPK*, *CHOP*, and the spliced isoform of X-box-binding protein-1 (*XBP1s*) in micropunches of the SFO. Near 2-fold elevations in all UPR biomarkers examined were found in the SFO (Figure 3B), indicative of robust ER stress in this circumventricular region during DIO. Based on these findings, further examination of the UPR in the SFO was conducted. In response to UPR activation, ER chaperones including GRP78 and protein disulfide

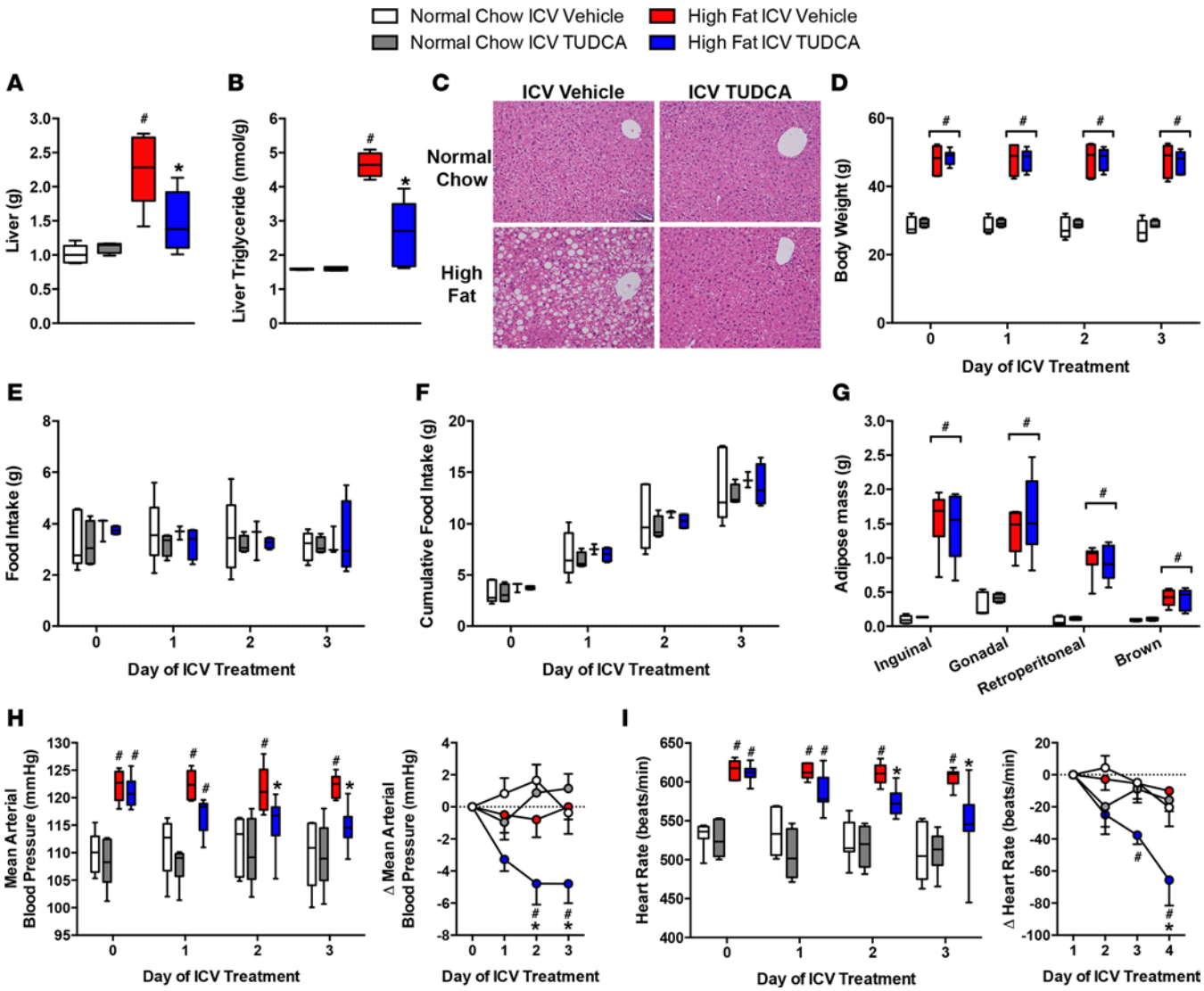

Figure 2. Short-term reductions in brain ER stress reduce obesity-induced hepatic steatosis, hypertension, and tachycardia independent of body weight, food intake, or adiposity. Liver mass (**A**) and hepatic triglyceride levels (**B**) following 3 days of daily intracerebroventricular (ICV) administration of the ER chemical chaperone TUDCA (to reduce ER stress) or vehicle in normal chow–fed and HFD-fed mice. n = 6–8. (**C**) H&E staining of the liver in mice that underwent ICV vehicle or TUDCA dosing. Representative of n = 4. Scale bar: 100 μm. Body weight (**D**), food intake (**E**), and cumulative food intake (**F**) in normal chow–fed and HFD-fed mice at baseline and during 3 days of ICV administration of TUDCA or vehicle. Regional adipose tissue mass (**G**) following 3 days of ICV vehicle or TUDCA administration. n = 6–8. Radiotelemetric measurements of mean arterial blood pressure (**H**) and heart rate (**I**) at baseline and during daily ICV TUDCA or vehicle administration. The respective change in blood pressure and heart rate is shown on the right (**H** and **I**). $^{\#}P < 0.05$ vs. normal chow groups; $^{*}P < 0.05$ vs. high fat ICV TUDCA. One-way or two-way repeated measures ANOVA. Box-and-whisker plots represent the median (line within box), upper and lower quartile (bounds of box), and maximum and minimum values (bars).

isomerase (PDI) were upregulated in the SFO, indicative of an attempt to counter HFD-induced ER stress (Figure 3C). Collectively, these findings indicate significant activation of the UPR in the SFO in response to HFD feeding.

In addition to activation of the UPR, ER stress results in ultrastructural alterations in the rough ER, including swelling and ribosomal detachment (24, 34). Therefore, electron microscopy was utilized to evaluate the ER ultrastructure in neuronal perikarya and large dendrites of the SFO in mice that were fed normal chow or HFD. The rough ER was graded as of normal appearance if: (i) substantial lengths of rough ER membrane were present; (ii) the rough ER membranes were parallel and showed no bloating; and (iii) substantial numbers of ribosomes were attached to the rough ER. Neuronal fragments were graded as showing ER stress if: (i) substantial lengths of rough ER were absent; (ii) the membranes of the rough ER were not parallel, and bloated segments or saccule-like fragments were present; and (iii) few or

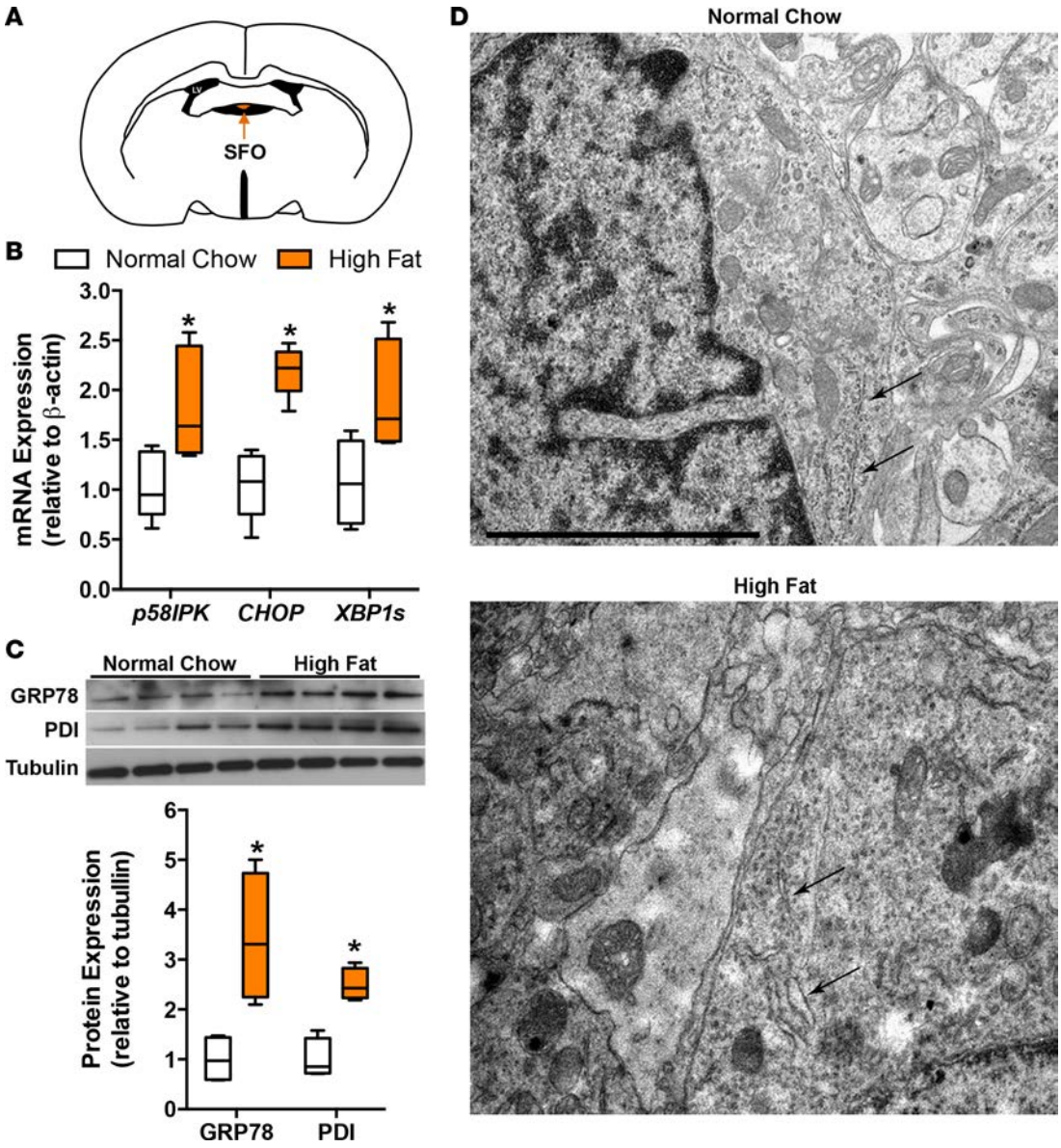

Figure 3. Obesity elicits robust UPR activation and ER ultrastructural alterations in the SFO. (**A**) Schematic highlighting the location of the SFO at the base of the lateral ventricle (LV). (**B**) Real-time PCR measurements of ER stress biomarkers *p58*^{IPK}, *CHOP*, and *XBP1s* from micropunches of the SFO in normal chow–fed or HFD-fed mice. $n = 5$. Two brains pooled per sample. (**C**) Western blot and quantitative summary of the ER chaperones GRP78 and PDI in SFO homogenates from normal chow–fed and HFD-fed mice. $n = 4$. Two brains pooled per sample. $^*P < 0.05$ vs. normal chow with a two-tailed unpaired *t*-test. Box-and-whisker plots represent the median (line within box), upper and lower quartile (bounds of box), and maximum and minimum values (bars). (**D**) Representative electron micrographs of rough ER (arrows) in SFO neurons of a normal chow–fed (left) and HFD-fed mouse (right). The electron micrographs are representative of 20–28 neuronal and dendritic fragments evaluated from 3 mice in each group. Scale bar = 2 μm

no ribosomes were seen attached to the rough ER. SFO rough ER from lean animals exhibited flat, tube-like cisternae with dense ribosomal attachment (Figure 3D, top). In contrast, ER in the SFO of obese animals appeared bloated or had saccule-like fragments with ribosomal detachment evident (Figure 3D, bottom). Thus, in addition to marked activation of the UPR, obesity is associated with alterations in rough ER morphology in SFO neurons.

SFO-ER stress mediates obesity-induced hepatic steatosis independent of changes in body weight, food intake, or adiposity. Our findings presented in Figures 1–3 indicate that brain ER stress mediates hepatic steatosis and that HFD feeding elicits marked ER stress in the circumventricular SFO. Interestingly, short-term ICV

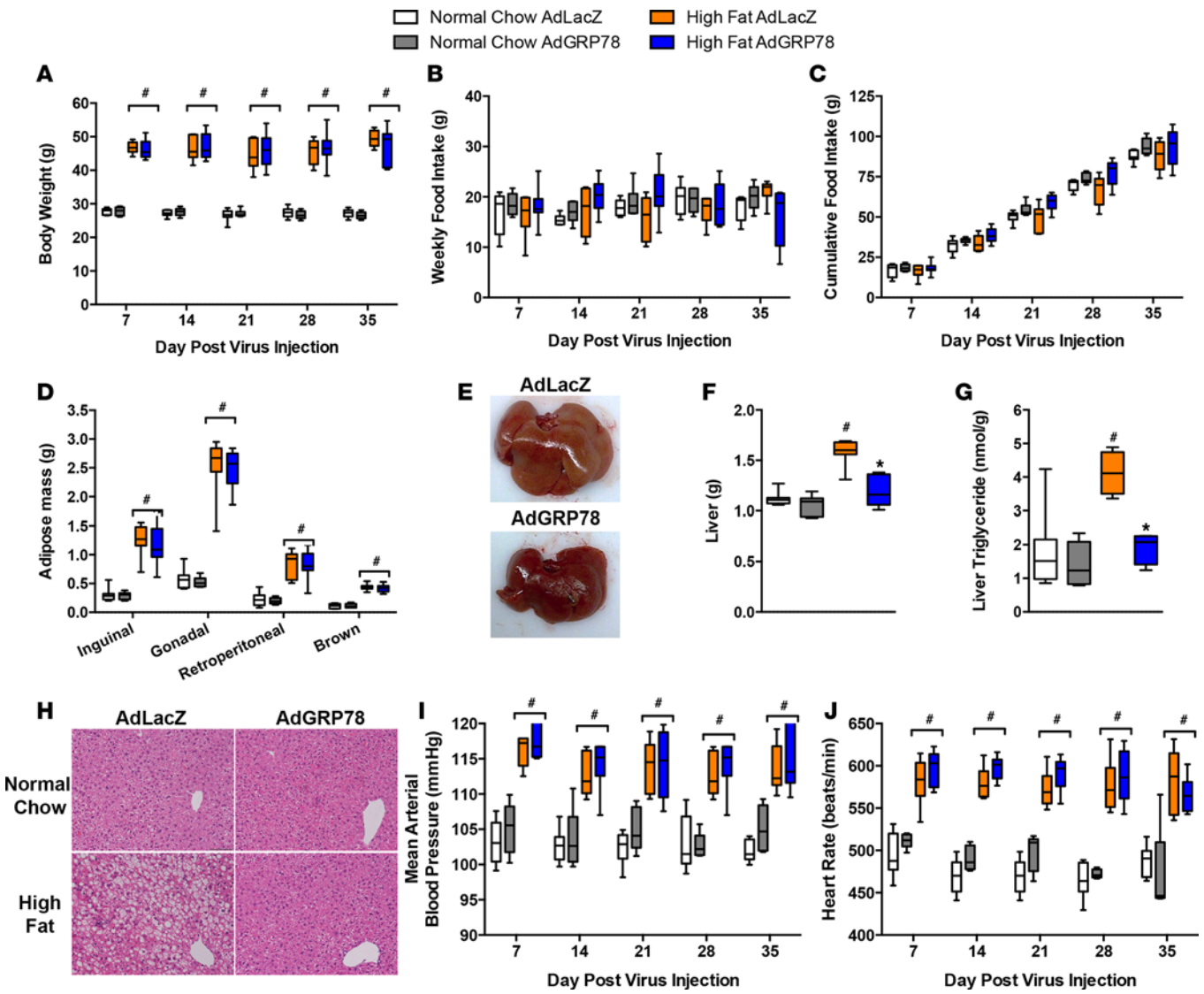

Figure 4. Selective reductions in SFO-ER stress rescue obesity-induced hepatic steatosis, independent of body weight, food intake, or adiposity. Body weight (**A**), food intake (**B**), and cumulative food intake (**C**) in normal chow–fed and HFD-fed mice following chronic SFO-targeted viral overexpression of the ER chaperone GRP78 (AdGRP78) or control vector (AdLacZ). Regional adipose tissue (**D**) mass 5 weeks after SFO-targeted AdGRP78 or AdLacZ. Representative liver images in HFD-fed mice (**E**), as well as liver mass (**F**) and hepatic triglyceride levels (**G**) in HFD-fed and normal chow–fed mice following SFO-targeted AdGRP78 or AdLacZ. n = 6–8. H&E staining (**H**) of the liver in mice 5 weeks after SFO-targeted AdGRP78 or AdLacZ. Representative of n = 4. Scale bar: 100 μm. Radiotelemetric measurements of mean arterial blood pressure (**I**) and heart rate (**J**) following adenoviral overexpression of GRP78, or control vector, in the SFO. $^{\#}P < 0.05$ vs. normal chow groups; $^{*}P < 0.05$ vs. high fat AdLacZ. One-way or two-way repeated measures ANOVA. Box-and-whisker plots represent the median (line within box), upper and lower quartile (bounds of box), and maximum and minimum values (bars).

administration of TUDCA reduced ER stress in the SFO of HFD-fed mice, as indicated by a 35%–40% reduction in UPR markers (Supplemental Figure 3B), suggesting that SFO-ER stress is functionally linked to hepatic steatosis in the context of obesity. To more specifically interrogate the SFO, we utilized an approach to genetically reduce ER stress selectively in the SFO. An effective means to prevent and rescue ER stress is via overexpression of the ER chaperone GRP78, which prevents downstream UPR activation (24, 35, 36). In this context, we recently developed an adenoviral vector that allows for overexpression of the full-length murine sequence of GRP78 (AdGRP78) (24). This vector includes an ER retention signal (KDEL) — which results in targeting of GRP78 to the ER, as demonstrated previously (24) — and is highlighted with transfection and immunohistochemical evaluation of Neuro2A neuronal cells (Supplemental Figure 4). Using this genetic approach, mice that had been fed normal chow or HFD for 15 weeks (starting at 6 weeks of age) underwent stereotaxic SFO–targeted AdGRP78 or control AdLacZ microinjections and were monitored for 5 weeks after adenoviral delivery. HFD-fed control vector mice

demonstrated significantly higher body weights than normal chow counterparts, and targeted overexpression of GRP78 in the SFO did not influence body weight in obese or lean animals (Figure 4A). Similarly, food intake over the 5-week study period was not different between control and AdGRP78-treated mice (Figure 4, B and C). Upon sacrifice, evaluation of regional adipose tissue mass revealed significant HFD-induced elevations in s.c. and visceral white adipose tissue, as well as subscapular brown fat mass (Figure 4D). These increases in adipose tissue were not altered by delivery of GRP78 to the SFO. Importantly, this lack of influence on body weight, food intake, and adiposity was not due to lack of functionality of the viral vector, as reductions in gene expression of UPR markers following SFO-targeted AdGRP78 were found, in concert with significant overexpression of the transgene (Supplemental Figure 5). Moreover, targeting of AdGRP78 to the SFO did not alter ER stress in other metabolic control regions, including the ventromedial hypothalamus and arcuate nucleus, highlighting that this approach was selective for the SFO (Supplemental Figure 5). These findings indicate that reducing ER stress in the SFO during established obesity does not influence body weight, food intake, or adiposity.

As shown in Figure 4E, livers from obese mice treated with the control vector were enlarged with a pale yellowish color. In sharp contrast, livers from SFO-targeted AdGRP78 obese animals exhibited a normal dark red color. In line with this, HFD feeding elicited significant hepatomegaly, which was rescued by selectively reducing ER stress in the SFO (Figure 4F). Measurement of hepatic triglycerides revealed significant steatosis in response to HFD feeding, and overexpression of GRP78 in the SFO of obese animals reduced liver triglycerides to normal chow levels (Figure 4G). This SFO-ER stress–associated influence on hepatic steatosis was also reflected at the histological level, with lipid droplet accumulation in the liver in response to HFD feeding being abrogated following targeted reductions in ER stress with AdGRP78 in the SFO (Figure 4H). No changes in liver weight or steatosis were found in normal chow mice treated with SFO-targeted AdGRP78 (Figure 4, F–H). Importantly, liver GRP78 mRNA and protein expression were not increased in normal chow or HFD mice following SFO-targeted AdGRP78 (Supplemental Figure 6), underscoring that the robust hepatic effects were due to SFO overexpression of GRP78. Collectively, these findings indicate that selectively reducing obesity-induced ER stress in the SFO rescues hepatic steatosis and hepatomegaly, independent of changes in body weight, food intake, or adiposity.

SFO-ER stress does not contribute to the maintenance of obesity-induced hypertension and tachycardia. As presented and discussed in Figure 2, H and I, short-term administration of the ER chemical chaperone TUDCA to globally reduce brain ER stress demonstrated a role for CNS UPR in the maintenance of obesity-induced hypertension and tachycardia. However, these studies did not permit selective evaluation of the brain regions involved. The SFO is crucial for cardiovascular regulation, and ER stress in this nucleus has been shown to underlie the development of angiotensin-II–mediated hypertension (24). Given this, along with our finding of SFO-ER stress–mediated hepatic steatosis (Figure 4, E–H), we reasoned that SFO-ER stress may also contribute to hypertension and tachycardia in DIO mice. Consistent with previous reports (21, 37) and Figure 2, H and I, 24-hour radiotelemetry recordings revealed significant elevations in arterial pressure and heart rate in DIO mice compared with lean, normal chow–fed counterparts (Figure 4, I and J). Surprisingly, adenoviral overexpression of GRP78 targeted to the SFO did not alter arterial pressure or heart rate in HFD-fed mice (Figure 4, I and J), suggesting that ER stress in this brain nucleus is not involved in obesity-induced cardiovascular changes. These data reveal a striking selectivity in the pathological consequence of SFO-ER stress in DIO, with a robust contribution to hepatic steatosis but a lack of an effect on arterial pressure, heart rate, food intake, body weight, and adiposity.

Discussion

We report here that brain ER stress has a direct role in mediating hepatic steatosis. First, short-term pharmacological induction of ER stress selectively in the CNS was sufficient to elicit a fatty liver phenotype without evidence of hepatic ER stress. Second, acute ER chemical chaperone–mediated alleviation of brain ER stress reduced obesity-associated elevations in hepatic triglycerides to normal levels. Third, hallmarks of ER stress including robust activation of the UPR and ER ultrastructural abnormalities were found in the forebrain circumventricular SFO in response to HFD feeding, and genetic reductions in ER stress selectively in this brain region rescued obesity-induced hepatomegaly and hepatic steatosis. Notably, these findings were independent of changes in body weight, adiposity, and caloric intake. In aggregate, these data identify a role for brain ER stress, notably within the SFO, as a key contributor to obesity-induced hepatic steatosis.

While significant progress has been made into the pathogenesis of NAFLD, the precise underlying mechanisms remain poorly understood. ER stress has emerged as a central factor in this process due to the close relationship between alterations in ER function and proposed contributing factors such as HFD, insulin resistance, inflammation, and oxidative stress (8–12, 15). While the focus has been on these mechanisms at the peripheral level, intriguingly, CNS UPR activation is emerging as a key contributor to obesity-related disorders (21–23). Based on this, we reasoned that brain ER stress may underlie NAFLD. Our findings using brain-specific induction of ER stress (Figure 1) or CNS-selective inhibition of obesity-induced ER stress (Figure 2) provide evidence that activation of the brain UPR can cause hepatomegaly and hepatic steatosis. The striking effect with only 3 days of ICV thapsigargin or TUDCA suggests a profound influence of CNS ER stress on NAFLD development, which appears to occur independently of hepatic ER stress.

It is likely in the setting of obesity and NAFLD that there are numerous contributors to brain ER stress, such as alterations in nutrient flux, inflammation, and lipotoxicity. In this regard, circumventricular regions such as the SFO, anatomically situated outside of the blood-brain-barrier, may be particularly susceptible to ER stress due to constant exposure to circulating ER stress–inducing factors. The SFO has recently emerged as a unique CNS area that is involved in integrative metabolic control (30, 32), so we reasoned that ER stress in the SFO may be a particularly relevant contributor to NAFLD. Indeed, selectively reducing UPR activation in the SFO resulted in a restoration of obesity-induced hepatomegaly and heaptic steatosis. While the underlying molecular mechanisms in the SFO that modulate hepatic lipid regulation remain to be determined, the SFO contains extensive efferent connections to brainstem and hypothalamic metabolic control regions (29–31). Thus, it is possible that ER stress in the SFO alters downstream CNS networks that influence liver metabolism through hormonal (i.e., insulin/glucagon) as well as autonomic nervous system control (17–20). Interestingly, an emerging body of literature suggests that CNS UPR activation leads to central leptin and insulin resistance (22, 38), and brain leptin and insulin signaling are tightly linked to hepatic metabolism (39–43). Therefore, it is also plausible that SFO-ER stress may contribute to NAFLD via disrupting CNS insulin and leptin signaling, although future studies are warranted in this regard, as is consideration of other nutrient-sensing components such as glucose and free fatty acids that are involved in hepatic control (44, 45).

In addition to contributing to NAFLD, obesity is also associated with an increased risk for the development of cardiovascular diseases, including hypertension (27, 28). Emerging evidence also indicates that nonobese hypertensive patients are prone to the development of NAFLD (46). While the interrelationships between hypertension and NAFLD are likely complex, we reasoned that brain ER stress may represent a common mechanism underlying both of these diseases. Indeed, we and others have shown that short-term increases in brain ER stress (i.e., thapsigargin) result in elevations in arterial pressure (21, 24). Conversely, here we show that globally reducing brain ER stress in obese animals lowers arterial pressure and heart rate during HFD, findings that are in support of previous work by Cai and colleagues (21). However, selective overexpression of GRP78 and reductions in HFD-induced ER stress biomarkers specifically in the SFO did not influence obesity-associated elevations in arterial pressure and heart rate. These findings were surprising, considering the SFO is well recognized to play a critical role in cardiovascular control (29–31) and ER stress in the SFO is directly involved in other forms of hypertension (e.g., angiotensin-II) (24). Taken together, our findings suggest that, while brain ER stress contributes to the maintenance of hypertension and tachycardia in obesity (i.e., ICV TUDCA), this is not due to UPR activation in the SFO. Of note, our studies were focused on conditions of established obesity, and therefore, we cannot rule out the possibility that ER stress in the SFO may contribute to the development of DIO-induced hypertension.

In parallel with revealing a role for the CNS in hepatic steatosis, the current findings also advance the concept of "uncoupling" of comorbid obesity conditions (37, 47). That is, obesity is associated with a spectrum of metabolic and cardiovascular disorders, raising the question as to whether these conditions are mechanistically coupled. In this context, previous work has suggested that discrete hypothalamic neuronal populations (POMC vs. AgRP) may contribute to hypertension and obesity independently, representing an "uncoupling" of these two conditions (37). Through selective targeting of SFO-ER stress, our findings build upon this work and demonstrate further CNS region-specific uncoupling of obesity-associated conditions. Specifically, targeting HFD-mediated ER stress in the SFO selectively rescued an NAFLD phenotype, without an effect on body weight, food intake, adiposity or hypertension. It is thus possible that discrete CNS nuclei and neuronal populations work as distributed interconnected and/or independent networks to contribute to obesity-related metabolic and cardiovascular diseases.

In summary, the current findings provide new evidence of an intriguing link between CNS ER stress and NAFLD. Notably, they reveal a role for the forebrain circumventricular SFO in the pathogenesis of hepatic steatosis. Moreover, these studies could fundamentally advance the way in which we think about hepatic disorders and suggest that interventions that regulate the brain UPR may represent new therapeutic opportunities for treating NAFLD.

Methods

Animals. Studies on the effects of acute chemical ER stress induction were conducted in adult (8–12 weeks old) male C57Bl/6 mice (Jackson Laboratory) fed standard chow (10% kcal fat, 70% carbohydrate, 20% protein; Research Diets Inc.) and provided water ad libitum. For DIO studies, C57Bl/6 mice were fed a HFD (60% fat, 20% carbohydrate, 20% protein) from 6 weeks of age for 15 weeks. Control animals for these studies remained on standard chow for the same period of time.

Pharmacological agents. The ER stress inducer thapsigargin (EMD Chemicals) was dissolved in 0.1% DMSO and diluted with saline to the desired concentration (1 μg in 1 μl). TUDCA (EMD Chemicals) was diluted in artificial cerebrospinal fluid (aCSF) (5 μg in 1 μl). The doses of TG and TUDCA have been confirmed extensively to induce or inhibit ER stress, respectively, in vivo (see also Supplemental Figure 1 and Supplemental Figure 3B) (21, 22, 24). The appropriate vehicle control was used for each pharmacological agent.

Arterial blood pressure and heart rate recording. For conscious recordings of arterial blood pressure and heart rate, mice were anesthetized (ketamine, 150 mg/kg, and xylazine, 15 mg/kg, i.p.) and instrumented with radiotelemetry probes (TA11PA-C10, Data Sciences International) as described (24, 48). Briefly, the telemetry catheter was implanted in the thoracic aorta via the left common carotid artery, the body of the radiotelemetry probe was placed in a right flank s.c. pocket, and the wound was closed and sutured. Body temperature was maintained at 37°C throughout surgical procedures and during recovery using a heating pad. For certain experiments, mice were instrumented for telemetry experiments in the same surgical session as adenoviral gene transfer and/or lateral cerebroventricular cannulation (see below). Mice remained undisturbed in their home cages for a minimum of 7 days to allow full recovery of normal circadian rhythm and cardiovascular parameters before obtaining recordings.

Lateral cerebroventricle cannulation and targeting of the SFO with adenoviral vectors. Mice were instrumented with an ICV cannula (PlasticsOne Inc.) for brain injection of pharmacological agents (24, 32, 33). Following anesthesia induction (ketamine, 150 mg/kg, and xylazine, 15 mg/kg, i.p.), mice were placed in a stereotaxic device and the surface of the skull was visualized under a dissecting microscope. A hole was drilled in the skull at the appropriate location, and the ICV cannula was slowly lowered into position (0.3 mm rostral, 1.0 mm lateral to Bregma, and 3.2 mm ventral from the dorsal surface of the skull). Two anchor eyepiece screws were placed posterior to the cannula, and dental cement was used to fix the cannula and screws in place. Mice were given a minimum of 7 days to the recover prior to ICV administration of pharmacological agents.

Recombinant adenoviral vectors encoding the full-length cDNA of mus musculus 78 kDa glucose-regulated protein (GenBank ID: NM_022310) (AdGRP78, 6 × 107 plaque-forming units/ml), and titer-matched AdLacZ were obtained from the Iowa Gene Transfer Vector Core. The construction and characterization of AdGRP78 has been described in detail previously (24). Briefly, a human Ad serotype 5 in which the E1a and E1b replication genes have been deleted was used, and GRP78 was driven under the control of the CMV promoter and in the same construct in the reporter gene β-galactosidase was driven off the RSV promoter. For SFO targeting of the adenoviral vectors, mice were anesthetized and placed in a stereotaxic device as above. The adenovirus was targeted to the SFO using a custom pressure injection system and pulled glass pipettes. The glass pipette tip was lowered 3.0 mm ventral from the dorsal surface of the skull at 0.3 mm rostral and 1.0 mm lateral to Bregma. The adenovirus was administered over a 4–5 minute period (500 nl). Mice were given a minimum of 7 days for surgical recovery. Using this method, we have shown highly localized, robust, and stable transgene expression in the SFO (24, 32, 49).

Quantitative PCR. Following euthanization by decapitation, mouse brains were removed and immediately placed on dry ice. Micropunches of individual brain nuclei were isolated based on anatomical locations as previously described (24, 32, 33). Tissue from two mice was pooled per biological sample in some studies. For other protocols, the brain was separated into forebrain, midbrain, and hindbrain segments and processed separately for each individual animal (Supplemental Figure 1). Total RNA was isolated by TRIzol (Invitrogen) extraction and converted to cDNA using a commercially available kit (Applied Biosystems). cDNA (25 ng) were subjected in triplicate to quantitative PCR (qPCR; ABI 7500

FAST system) using Power SYBR Green (Applied Biosystems). All primers were derived from mus musculus (National Center for Biotechnology Information GenBank). Primer sequences used were: p58IPK F: 5′-GTGGCATCCAGATAATTTCCAG-3′, R: 5′-GAGTTCCAACTTCTGTGGAAGG-3; CHOP F: 5′-ATATCTCATCCCCAGGAAACG-3′, R: 5′-TCTTCCTTGCTCTTCCTCCTC-3′; GRP78 F: 5′- TTCAGCTGTCACTCGGAGAAT-3′, R: 5′- ATATCTCATCCCCAGGAAACG -3′; XBP1s F: 5′- GAGTCCGCAGCAGGTG -3′, R: 5′- GTGTCAGAGTCCATGGGA -3′; GRP94 F: 5′-CTCAGAAGACGCAGAAGACTCA-3′, R: 5′- AAAACTTCACATTCCCTCTCCA -3′; β-actin F: 5′-CATCCTCTTCCTCCCTGGAGAAGA-3′, R: 5′-ACAGGATTCCATACCCAAGAAGGAAGG-3′; 18s F: 5′- GTAACCCGTTGAACCCCATT-3′, R: 5′- CCATCCAATCGGTAGTAGCG-3′.

β-Actin or 18s were used as calibrator genes in all experiments. The average expressed isoform of each experimental gene was expressed relative to the calibrator, and the relative fold change compared with the calibrator was calculated using the comparative ΔΔCt method (50).

Western blot. Micropunches of the SFO were isolated, and two mice were pooled per biological sample. Protein was isolated in mammalian tissue lysis buffer (Sigma-Aldrich) with protease inhibitor (Sigma-Aldrich). Western analyses for GRP78 and PDI were performed using standard procedures, and protein levels were expressed relative to tubulin. Protein (15 μg) was loaded per sample lane, and GRP78 (1:10,000), PDI (1:5,000), and tubulin (1:10,000) antibodies (Cell Signaling Technology) were used. Similar procedures were used to examine liver GRP78 (1:1,000) and were expressed relative to GAPDH (1:50,000; AbCam).

IHC. Cultured Neuro2A cells were transfected with AdGRP78, and IHC was performed 24 hours later by fixing cells at 80% confluence for 20 minutes at room temperature with 4% paraformaldehyde (PFA) in 1× PBS. Cells were then washed twice with 1× PBS followed by sequential incubation with primary antibodies for GRP78 (1:200, Abcam) and the ER protein calnexin (1:100, Santa Cruz Biotechnology Inc.). Cells were subsequently incubated in Alexa-Fluor–conjugated antibodies (Invitrogen) in 0.1 Triton X-100 and 1× PBS buffer. DAPI was used as a counterstain, and slides were mounted with Prolong Gold Antifade. Images were obtained with a Zeiss Axio Imager.

Ultrastructural analysis of rough ER in SFO neurons. Male C57Bl/6 mice fed normal chow (n = 3) or HFD (n = 3) for 15 weeks starting at 6 weeks of age were anesthetized and transcardially perfused with 0.9% saline followed by an ice-cold fixative consisting of 1% glutaraldehyde and 4% PFA in phosphate buffer (pH 7.2, 0.167 M). Brains were removed and cut into 50-μm thick coronal sections. Sections containing the SFO were osmicated (0.5% osmic acid in distilled water), dehydrated in acetone, and flat-embedded in Epon 812 (Electron Microscopy Sciences). Under a dissecting microscope, the embedded SFO was cut out from 3 or 4 sampled sections from each animal and mounted on Epon bullets (Electron Microscopy Services). Ultrathin sections were cut with a diamond knife, mounted on Formvar-coated grids, stained with uranyl acetate and lead citrate, and examined using a JEOL 1230 electron microscope. At least five grids from each sampled section from each animal were examined, and neuronal perikarya and large dendrites containing identifiable segments of rough ER were photographed. The rough ER in neuronal fragments was graded as described in detail in the Results.

Hepatic triglyceride measurements. Livers were flash frozen on dry ice and stored at –80°C. Hepatic triglycerides were extracted and quantified using a triglyceride colorimetric assay kit (Biovision) according to the manufacturer's protocol. Briefly, liver tissue (~50 mg) was homogenized in 5% Triton X-100, followed by heating in a water bath at 90°C for 5 minutes. After cooling to room temperature, insoluble cellular components were removed by microcentrifugation for 2 minutes. The diluted sample supernatant was combined with a triglyceride probe, enzyme mix, and lipase (all supplied by Biovision, Inc.), and absorbance was measured at 570 nm in a microtiter plate reader (Varioskan Flash, Thermo Fisher Scientific). Blank and lipase controls were subtracted from the optical density of each sample to allow for the quantification of triglycerides. Triglyceride concentrations were interpolated from the linear regression of a standard curve and normalized by the wet weight of liver tissue used in the assay.

Liver histology. Livers were obtained upon sacrifice and immediately placed in 10% formalin overnight. The tissue was paraffin embedded and then sectioned at 5 μm. H&E staining was performed using standard procedures. Images were obtained using an Olympus BX43 inverted fluorescent microscope.

Statistics. Data are expressed as mean ± SEM. Two-tailed unpaired t tests were used for comparisons between two groups. Multiple comparisons were evaluated using an appropriate ANOVA (one-way or two-way repeated measures). Post-hoc comparisons were performed with a Tukey's post-hoc comparison when significant main effects were detected. Significance was set at $P < 0.05$.

Study approval. All procedures were approved by the Animal Care and Use Committees at Cornell University, The University of Iowa, and the George Washington University. Care of the mice met the standards set forth by the NIH *Guide for the Care and Use of Laboratory Animals* (National Academies Press, 2011).

Author contributions

CNY, ALM, and RLD designed the studies. JAH, CH, SDB, MG, MDC, and CNY performed and analyzed the experiments. CNY, ALM, and RLD wrote the manuscript. All authors participated in important discussion of the data, edited the paper and approved the manuscript.

Acknowledgments

This work was supported by NIH grants HL116776 (CNY) and HL084207 (ALM and RLD) and by research funds from the Roy J. Carver Trust (ALM). We would like to thank Daniel Ho for technical assistance.

Address correspondence to: Colin N. Young, 2300 Eye Street NW, 448 Ross Hall, The George Washington University, Washington, DC 20037, USA. Phone: 202.994.9575; E-mail: colinyoung@gwu.edu.

1. Angulo P. Obesity and nonalcoholic fatty liver disease. *Nutr Rev*. 2007;65(6 Pt 2):S57–S63.
2. Browning JD, et al. Prevalence of hepatic steatosis in an urban population in the United States: impact of ethnicity. *Hepatology*. 2004;40(6):1387–1395.
3. Cohen JC, Horton JD, Hobbs HH. Human fatty liver disease: old questions and new insights. *Science*. 2011;332(6037):1519–1523.
4. Browning JD, Horton JD. Molecular mediators of hepatic steatosis and liver injury. *J Clin Invest*. 2004;114(2):147–152.
5. Bedogni G, Miglioli L, Masutti F, Tiribelli C, Marchesini G, Bellentani S. Prevalence of and risk factors for nonalcoholic fatty liver disease: the Dionysos nutrition and liver study. *Hepatology*. 2005;42(1):44–52.
6. Falck-Ytter Y, Younossi ZM, Marchesini G, McCullough AJ. Clinical features and natural history of nonalcoholic steatosis syndromes. *Semin Liver Dis*. 2001;21(1):17–26.
7. Treeprasertsuk S, Leverage S, Adams LA, Lindor KD, St Sauver J, Angulo P. The Framingham risk score and heart disease in nonalcoholic fatty liver disease. *Liver Int*. 2012;32(6):945–950.
8. Malhi H, Kaufman RJ. Endoplasmic reticulum stress in liver disease. *J Hepatol*. 2011;54(4):795–809.
9. Zhang XQ, Xu CF, Yu CH, Chen WX, Li YM. Role of endoplasmic reticulum stress in the pathogenesis of nonalcoholic fatty liver disease. *World J Gastroenterol*. 2014;20(7):1768–1776.
10. Oyadomari S, Harding HP, Zhang Y, Oyadomari M, Ron D. Dephosphorylation of translation initiation factor 2alpha enhances glucose tolerance and attenuates hepatosteatosis in mice. *Cell Metab*. 2008;7(6):520–532.
11. Ozcan U, et al. Chemical chaperones reduce ER stress and restore glucose homeostasis in a mouse model of type 2 diabetes. *Science*. 2006;313(5790):1137–1140.
12. Hotamisligil GS. Endoplasmic reticulum stress and the inflammatory basis of metabolic disease. *Cell*. 2010;140(6):900–917.
13. Zhang K, Kaufman RJ. From endoplasmic-reticulum stress to the inflammatory response. *Nature*. 2008;454(7203):455–462.
14. Lee J, Ozcan U. Unfolded protein response signaling and metabolic diseases. *J Biol Chem*. 2014;289(3):1203–1211.
15. Ozcan U, et al. Endoplasmic reticulum stress links obesity, insulin action, and type 2 diabetes. *Science*. 2004;306(5695):457–461.
16. Malhotra JD, Kaufman RJ. Endoplasmic reticulum stress and oxidative stress: a vicious cycle or a double-edged sword? *Antioxid Redox Signal*. 2007;9(12):2277–2293.
17. Shimazu T. Progress and perspective of neuro-hepatology. In: Shimazu T, ed. *Liver innervation and neural control of hepatic function*. Eastleigh: John Libbey & Company Ltd; 1996:3–13.
18. Kalsbeek A, Bruinstroop E, Yi CX, Klieverik LP, La Fleur SE, Fliers E. Hypothalamic control of energy metabolism via the autonomic nervous system. *Ann N Y Acad Sci*. 2010;1212:114–129.
19. Gardemann A, Püschel GP, Jungermann K. Nervous control of liver metabolism and hemodynamics. *Eur J Biochem*. 1992;207(2):399–411.
20. Geerling JJ, et al. Sympathetic nervous system control of triglyceride metabolism: novel concepts derived from recent studies. *J Lipid Res*. 2014;55(2):180–189.
21. Purkayastha S, Zhang H, Zhang G, Ahmed Z, Wang Y, Cai D. Neural dysregulation of peripheral insulin action and blood pressure by brain endoplasmic reticulum stress. *Proc Natl Acad Sci USA*. 2011;108(7):2939–2944.
22. Zhang X, Zhang G, Zhang H, Karin M, Bai H, Cai D. Hypothalamic IKKbeta/NF-kappaB and ER stress link overnutrition to energy imbalance and obesity. *Cell*. 2008;135(1):61–73.
23. Cai D, Liu T. Inflammatory cause of metabolic syndrome via brain stress and NF-κB. *Aging (Albany NY)*. 2012;4(2):98–115.
24. Young CN, et al. ER stress in the brain subfornical organ mediates angiotensin-dependent hypertension. *J Clin Invest*. 2012;122(11):3960–3964.
25. Wofford MR, Hall JE. Pathophysiology and treatment of obesity hypertension. *Curr Pharm Des*. 2004;10(29):3621–3637.
26. Davy KP, Hall JE. Obesity and hypertension: two epidemics or one? *Am J Physiol Regul Integr Comp Physiol*. 2004;286(5):R803–R813.
27. Brookes MJ, Cooper BT. Hypertension and fatty liver: guilty by association? *J Hum Hypertens*. 2007;21(4):264–270.
28. Dixon JB, Bhathal PS, O'Brien PE. Nonalcoholic fatty liver disease: predictors of nonalcoholic steatohepatitis and liver fibrosis in the severely obese. *Gastroenterology*. 2001;121(1):91–100.
29. Cottrell GT, Ferguson AV. Sensory circumventricular organs: central roles in integrated autonomic regulation. *Regul Pept*.

2004;117(1):11–23.
30. Mimee A, Smith PM, Ferguson AV. Circumventricular organs: targets for integration of circulating fluid and energy balance signals? *Physiol Behav*. 2013;121:96–102.
31. Smith PM, Ferguson AV. Circulating signals as critical regulators of autonomic state--central roles for the subfornical organ. *Am J Physiol Regul Integr Comp Physiol*. 2010;299(2):R405–R415.
32. Young CN, et al. Angiotensin type 1a receptors in the forebrain subfornical organ facilitate leptin-induced weight loss through brown adipose tissue thermogenesis. *Mol Metab*. 2015;4(4):337–343.
33. Young CN, Morgan DA, Butler SD, Mark AL, Davisson RL. The brain subfornical organ mediates leptin-induced increases in renal sympathetic activity but not its metabolic effects. *Hypertension*. 2013;61(3):737–744.
34. Ron D, Walter P. Signal integration in the endoplasmic reticulum unfolded protein response. *Nat Rev Mol Cell Biol*. 2007;8(7):519–529.
35. Kammoun HL, et al. GRP78 expression inhibits insulin and ER stress-induced SREBP-1c activation and reduces hepatic steatosis in mice. *J Clin Invest*. 2009;119(5):1201–1215.
36. Contreras C, et al. Central ceramide-induced hypothalamic lipotoxicity and ER stress regulate energy balance. *Cell Rep*. 2014;9(1):366–377.
37. Purkayastha S, Zhang G, Cai D. Uncoupling the mechanisms of obesity and hypertension by targeting hypothalamic IKK-β and NF-κB. *Nat Med*. 2011;17(7):883–887.
38. Schneeberger M, et al. Mitofusin 2 in POMC neurons connects ER stress with leptin resistance and energy imbalance. *Cell*. 2013;155(1):172–187.
39. Obici S, Zhang BB, Karkanias G, Rossetti L. Hypothalamic insulin signaling is required for inhibition of glucose production. *Nat Med*. 2002;8(12):1376–1382.
40. Obici S, Feng Z, Karkanias G, Baskin DG, Rossetti L. Decreasing hypothalamic insulin receptors causes hyperphagia and insulin resistance in rats. *Nat Neurosci*. 2002;5(6):566–572.
41. Brüning JC, et al. Role of brain insulin receptor in control of body weight and reproduction. *Science*. 2000;289(5487):2122–2125.
42. Könner AC, et al. Insulin action in AgRP-expressing neurons is required for suppression of hepatic glucose production. *Cell Metab*. 2007;5(6):438–449.
43. Cohen P, et al. Selective deletion of leptin receptor in neurons leads to obesity. *J Clin Invest*. 2001;108(8):1113–1121.
44. Lam TK, Schwartz GJ, Rossetti L. Hypothalamic sensing of fatty acids. *Nat Neurosci*. 2005;8(5):579–584.
45. Ogunnowo-Bada EO, Heeley N, Brochard L, Evans ML. Brain glucose sensing, glucokinase and neural control of metabolism and islet function. *Diabetes Obes Metab*. 2014;16 Suppl 1:26–32.
46. Donati G, et al. Increased prevalence of fatty liver in arterial hypertensive patients with normal liver enzymes: role of insulin resistance. *Gut*. 2004;53(7):1020–1023.
47. Rahmouni K, Davisson RL, Sigmund CD. Inflaming hypothalamic neurons raises blood pressure. *Cell Metab*. 2011;14(1):3–4.
48. Cao X, et al. Angiotensin II-dependent hypertension requires cyclooxygenase 1-derived prostaglandin E2 and EP1 receptor signaling in the subfornical organ of the brain. *Hypertension*. 2012;59(4):869–876.
49. Sinnayah P, Lindley TE, Staber PD, Cassell MD, Davidson BL, Davisson RL. Selective gene transfer to key cardiovascular regions of the brain: comparison of two viral vector systems. *Hypertension*. 2002;39(2 Pt 2):603–608.
50. Livak KJ, Schmittgen TD. Analysis of relative gene expression data using real-time quantitative PCR and the 2(-Delta Delta C(T)) Method. *Methods*. 2001;25(4):402–408.